Control of Phase in Phosphide Nanoparticles Produced by Metal Nanoparticle Transformation: Fe_2P and FeP

Elayaraja Muthuswamy,[†] Parashu Ram Kharel,[‡] Gavin Lawes,[‡] and Stephanie L. Brock[†,*]

[†]Department of Chemistry, Wayne State University, Detroit, Michigan 48202, and [‡]Department of Physics and Astronomy, Wayne State University, Detroit, Michigan 48201

ABSTRACT The transformation of Fe nanoparticles by trioctylphosphine (TOP) to phase-pure samples of either Fe_2P or FeP is reported. Fe nanoparticles were synthesized by the decomposition of $Fe(CO)_5$ in a mixture of octadecene and oleylamine at 200 °C and were subsequently reacted with TOP at temperatures in the region of 350−385 °C to yield iron phosphide nanoparticles. Shorter reaction times favored an iron-rich product (Fe_2P), and longer reaction times favored a phosphorus-rich product (FeP). The reaction temperature was also a crucial factor in determining the phase of the final product, with higher temperatures favoring FeP and lower temperatures Fe_2P. We also observe the formation of hollow structures in both FeP spherical nanoparticles and Fe_2P nanorods, which can be attributed to the nanoscale Kirkendall effect. Magnetic measurements conducted on phase-pure samples suggest that ~8 × 70 nm Fe_2P rods are ferromagnetic with a Curie temperature between 215 and 220 K and exhibit a blocking temperature of 179 K, whereas FeP is metamagnetic with a Néel temperature of ~120 K. These data agree with the inherent properties of bulk-phase samples and attest to the phase purity that can be achieved by this method.

KEYWORDS: iron phosphides · nanoparticles · synthesis · magnetic properties · structure transformation

Research efforts on nanoscale systems have risen exponentially during the past decade because of the unique and, for some applications, superior properties exhibited by nanomaterials compared to their bulk counterparts. High catalytic activity, superparamagnetism, and quantum confinement are among the notable properties that can be achieved in nanosized systems. Transition metal phosphides are an interesting class of materials and worth investigating on the nanoscale because of their wide scope of properties and applications.[1] Among these, iron phosphides and their ternary phases have been targeted for their magnetic characteristics, which include ferromagnetism, magnetoresistance, and magneto-caloric effects.[2,3] However, iron phosphides exist in a wide range of stoichiometries including Fe_3P, Fe_2P, FeP, FeP_2, and FeP_4, and the properties depend sensitively on their physical and electronic structure.[4−7] Thus, Fe_3P and Fe_2P are ferromagnetic, FeP is metamagnetic, and FeP_2 and FeP_4 are diamagnetic semiconductors. These properties are expected to vary with size and shape when prepared on the nanoscale, opening up new avenues of investigation and potential applications. Thus, significant effort has been applied toward the synthesis of iron phosphides on the nanoscale, but the factors that determine the specific phases generated are not well-documented, and the purity of some of the phases reported has been debated.

The synthesis of FeP nanoparticles was first reported by our group from reaction of $Fe(acac)_3$ with $P(SiMe_3)_3$ in trioctylphosphineoxide (TOPO) at 280 °C.[8] However, decomposition of organometallic species to generate transition metal species and the use of alkyl phosphines, like trioctylphosphine (TOP), as the phosphorus source has proven to be a more general and less expensive route to transition metal phosphide nanoparticles.[4,9] Thus, Hyeon and coworkers reported the synthesis of both FeP[10] and Fe_2P[11] nanorods by the continuous injection of $Fe(CO)_5$ and TOP using a syringe pump into hot surfactant/solvent systems. When the Fe−TOP complex was injected into a mixture containing oleylamine and octylether maintained at 300 °C, they were able to obtain Fe_2P nanorods, whereas when oleylamine and octylether were replaced with TOPO and the system aged at 360 °C, FeP nanorods were generated. The formation of a phosphorus-rich product in the latter case was attributed to the combination of TOPO and TOP resulting in a phosphorus-rich environment.[10] Using a similar system to that reported by Hyeon

*Address correspondence to sbrock@chem.wayne.edu.

Received for review June 1, 2009 and accepted July 28, 2009.

Published online August 4, 2009.
10.1021/nn900574r CCC: $40.75

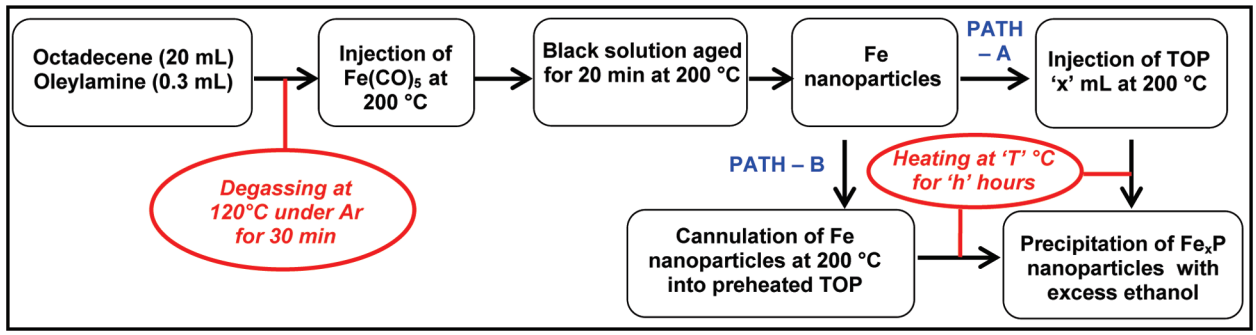

Scheme 1. Synthesis of Fe nanoparticles and subsequent conversion to Fe_xP nanoparticles.

for FeP, Liu[12] and co-workers showed that FeP nanorods and nanowires could also be accessed at lower temperatures (300 °C), and Chi[13] and co-workers showed that a different precursor, (η^4-cyclohexadiene)irontricarbonyl, also yields FeP nanowires with TOP at 360 °C. Very recently, the Whitmire[14] group used a single source precursor containing Fe/P in the ratio 3:1 with the aim of maintaining the ratio of the molecular precursor in the product. However, the decomposition of the precursor at 315−330 °C resulted in Fe_2P nanorods instead of the expected product, Fe_3P. Finally, Schaak[15−18] and co-workers transformed a variety of transition metal nanoparticles into their respective phosphide phases by reacting them with TOP. In particular, FeP nanoparticles were prepared by reacting Fe nanoparticles with TOP in hexadecylamine (HDA) at 360 °C.[16]

A similarity in many of the methods was the use of TOP as a nonstoichiometric precursor and cosolvent. Although some of the above methods have purported to result in phase-pure products, careful examination of powder X-ray diffraction (PXRD) patterns, as well as contradictory magnetic properties, suggests the presence of secondary phases.[10,13] Unfortunately, attempts to control stoichiometry using more reactive phosphines or single-source molecular precursors have not proven to be effective either.[14] In order to be able to target desired phases and gain an accurate estimation of the magnetic properties of nanoscale iron phosphides, a detailed study of the parameters that govern phase formation is needed.

Our objectives are to (i) determine the role of various synthetic parameters on the phase of Fe_xP generated, (ii) apply these methods to the formation of narrow polydispersity samples that are phase pure, and (iii) determine the intrinsic physicochemical properties of the iron phosphides as a function of phase on the nanoscale. We employed the generalized approach to prepare transition metal phosphide nanoparticles reported by Schaak and co-workers.[15−18] Fe nanoparticles were prepared first and then converted to the phosphide phase by reacting them with TOP. The role of temperature, amount of Fe and phosphorus precursors, and reaction duration in determining the final phase of the Fe_xP nanoparticles will be discussed, and the intrinsic magnetic properties of FeP and Fe_2P described.

RESULTS AND DISCUSSION

Fe_xP nanoparticles were prepared by conversion of preformed Fe nanoparticles with TOP at elevated temperatures, as summarized in Scheme 1. Spherical Fe nanoparticles were synthesized using the method reported by Sun and co-workers[19] by injecting $Fe(CO)_5$ into a degassed mixture of octadecene and oleylamine maintained at 200 °C. Within a few minutes, the system changed from colorless to black, indicating the formation of Fe nanoparticles. TEM analyses of aliquots taken from the reaction system of Fe nanoparticles after 20 min indicated formation of spherical nanoparticles with a core−shell structure (Figure 1a and Supporting Information). The shell can be attributed to the surface oxidation of reactive Fe nanoparticles during isolation.[20] A size distribution plot (Supporting Information) for these nanoparticles indicates that they are nearly monodisperse with an average size of 15.0 ± 0.7 nm (core plus shell). In line with the literature reports, the PXRD pattern of the Fe nanoparticles is featureless, indicating that they are amorphous (Supporting Information).[19] The isolated nanoparticles are attracted to the magnetic stir bar, consistent with formation of a ferromagnetic phase (Fe or Fe oxide).

In situ conversion of the Fe nanoparticles (aged for 20 min) into phosphide phases was initiated by either injection of TOP into the Fe nanoparticle system at 200 °C followed by raising the temperature to 350−385 °C for time intervals of 1 h to several days (Scheme 1, PATH-A) or cannulation of the Fe nanoparticles at 200 °C into preheated TOP maintained at 350−370 °C (Scheme 1, PATH-B). A series of reactions were conducted in which reaction temperature, reaction time, and Fe and P precursor amounts were independently varied in order to discern the key parameters governing phase formation and transformation within the Fe_xP nanoparticle system and the optimal conditions to prepare phase-pure samples.

Effect of Time at 350 °C: Reaction Series I. As a phosphorus source, TOP is relatively inert, requiring high temperature for activation (presumably by P−C bond cleavage)

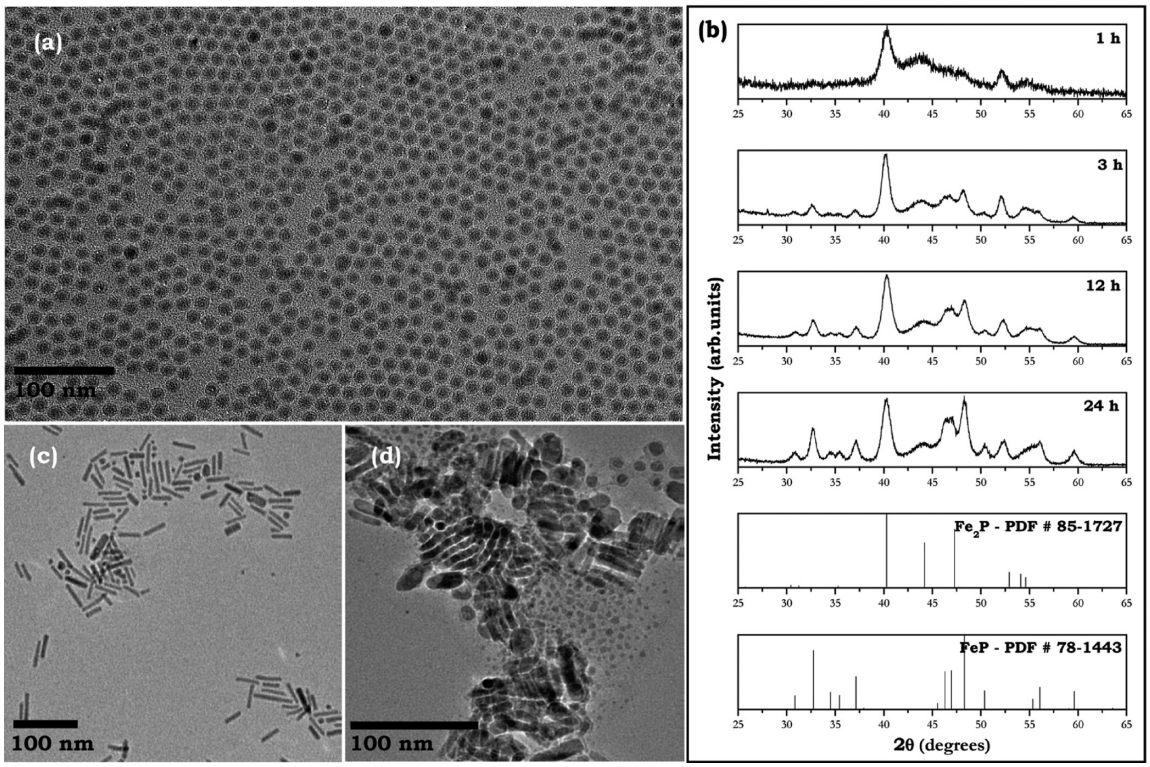

Figure 1. (a) TEM image of Fe nanoparticles aged for 20 min at 200 °C. (b) Reaction series I: PXRD patterns of the product from PATH-A (Scheme 1) as a function of heating time at 350 °C, compared to reference patterns for FeP and Fe_2P; TEM images of the Fe_xP nanoparticles after (c) 1 h and (d) 24 h.

and producing a lower yield of active phosphorus relative to $P(SiMe_3)_3$ (activation by P−Si bond cleavage and employed as a stoichiometric reagent).[8] Accordingly, we hypothesized that the amount of active phosphorus available to react with Fe nanoparticles could be manipulated by adjusting the temperature and the reaction duration. In order to test this hypothesis, we started the conversion reactions at 350 °C and varied the heating time from 1 to 24 h. The PXRD patterns for the final products are given in Figure 1b. The PXRD pattern of the 1 h sample indicated formation of a poorly crystalline material with broad peaks that can be indexed largely to Fe_2P. The samples made at longer heating times were characterized to be a mixture of both Fe_2P and FeP, with the former being the major product at short reaction times and the relative amount of the latter going up with increasing reaction time. The specific quantities of Fe_2P and FeP were not determined because we find that even small variations in reaction setup (using a different mantle or temperature probe) result in different relative quantities of the two species. Nevertheless, the trends observed, which are the focus of this investigation, are completely reproducible, and this is the first report of Fe_2P formation by the nanoparticle conversion route developed by Schaak and co-workers.[18]

With respect to morphology, products of the 1 h reaction were found to consist mostly of rods (Figure 1c), whereas the samples heated for longer times were found to be a mixture of both rods and spherical particles (Figure 1d). The change in morphology of the particles may be attributed to the gradual change of the reaction product from the Fe-rich product to a P-rich product. While orthorhombic FeP nanoparticles can be prepared as either spherical particles[8] or rods growing perpendicular to the (011) or (013) planes,[10,12] depending on reaction conditions; hexagonal Fe_2P nanoparticles are reported to favor formation of nanorods with preferential growth along the [001] axis.[10,11,14] Hollow structures were also apparent in the spherical particles as well as the rods, similar to the Ni_2P hollow structures reported by Schaak and co-workers[15,16] and Chiang and co-workers.[21] The formation of hollow structures is attributed to the nanoscale Kirkendall effect occurring due to the difference in the diffusion rates of Fe ions outward and P ions inward. At short times (1 h), the products are strongly attracted to a stir bar. On the basis of the fact that neither Fe_2P nor FeP is expected to be ferromagnetic at room temperature, this suggests that iron conversion is incomplete. In contrast, particles isolated after 3 h or longer were no longer attracted to a magnetic stir bar, suggesting the iron had completely reacted.

Effect of Precursor Concentration (TOP and $Fe(CO)_5$): Reaction Series II and III. We next explored the possibility that the precursor concentrations play a role in determining the phase and phase purity of the final product. During the conversion, we first varied the amount of TOP from 2.5 to 26.5 mL (5.6 to 59.4 mmol) while heating for

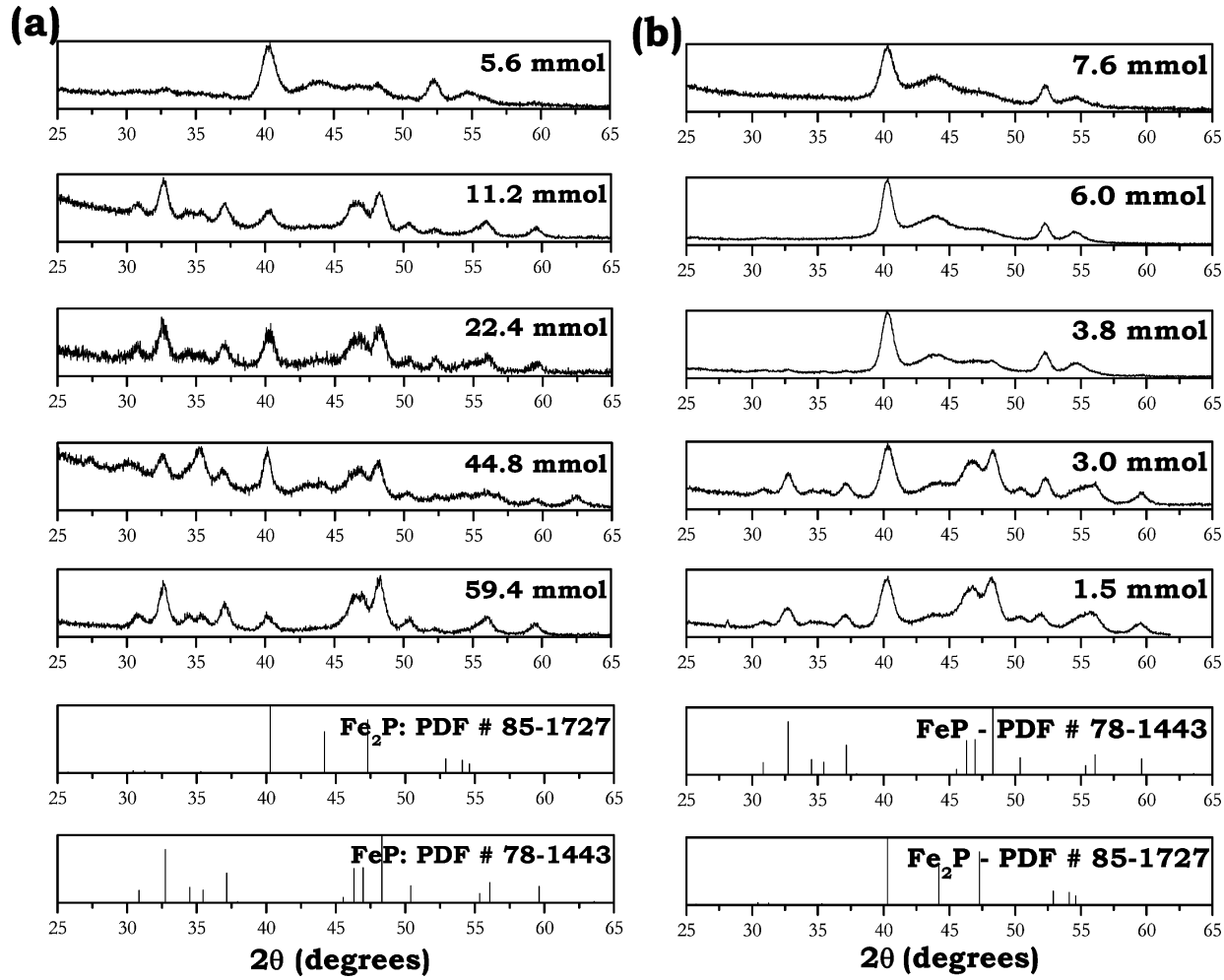

Figure 2. (a) Reaction Series II: PXRD patterns of the products from PATH-A (Scheme 1) as a function of TOP quantity; reactions were carried out at 350 °C for 24 h with 0.35 mL (2.7 mmol) $Fe(CO)_5$. (b) Reaction Series III: PXRD patterns of the products from PATH-A (Scheme 1) as a function of $Fe(CO)_5$ quantity; reactions were carried out at 350 °C for 6 h with 10 mL (22.4 mmol) TOP.

24 h at 350 °C. PXRD data suggested a mixture of phases with varying compositions of Fe_2P/FeP (Figure 2a). At low concentrations of TOP (5.6 mmol) the Fe-rich product (Fe_2P) was favored, whereas FeP formation was favored when more TOP was used in the reaction, suggesting a higher concentration of "available" phosphorus can drive conversion of Fe and/or Fe_2P to FeP. However, even for very large TOP amounts, Fe_2P remains a significant byproduct.

We also varied the concentration of Fe precursor, $Fe(CO)_5$, keeping all other reaction parameters constant, with the expectation that increasing the available iron would favor the Fe-rich product (Fe_2P). The PXRD patterns of the final products are given in Figure 2b. For 0.4 mL (3 mmol) of $Fe(CO)_5$ or lower, the final product was indexed to both FeP and Fe_2P phases, whereas the samples made with higher amounts of $Fe(CO)_5$ (0.8 mL, 6 mmol and 1.0 mL, 7.6 mmol) could be uniquely indexed to the Fe_2P phase. Presumably, increasing the precursor molar ratio of Fe/P from 0.067 to 0.34 results in a higher concentration of Fe nanoparticles and thereby promotes formation of the Fe-rich product (Fe_2P) while simultaneously eliminating the phosphorus-rich product (FeP).

Optimal Conditions for Phase-Pure Fe_2P Nanoparticles and Magnetic Properties. Despite appearing "PXRD pure", the 6 h Fe_2P samples prepared with $\geq$0.8 mL of $Fe(CO)_5$ were found to respond to a magnet at room temperature, suggesting the possible presence of unconverted Fe nanoparticles in the final product. To enable complete conversion to the iron-rich phosphide phase (Fe_2P), reactions were carried out for a longer duration (24 h) with an intermediate amount of $Fe(CO)_5$ (0.7 mL, 5.3 mmol) and 5 mL (11.2 mmol) of TOP. The PXRD pattern (Figure 3a) of the sample again matches well with the reference pattern for Fe_2P, but the sample is not attracted to the stir bar, suggesting conversion is complete in this case. TEM images (Figure 3b and Supporting Information) of the final product indicated that the sample consisted mainly of rods of varying lengths (40 to 110 nm) with an average width of 8 nm. A small number of near spherical particles was also observed.

The magnetization (M) as a function of temperature (T) for Fe_2P nanorods was measured using zero-field-

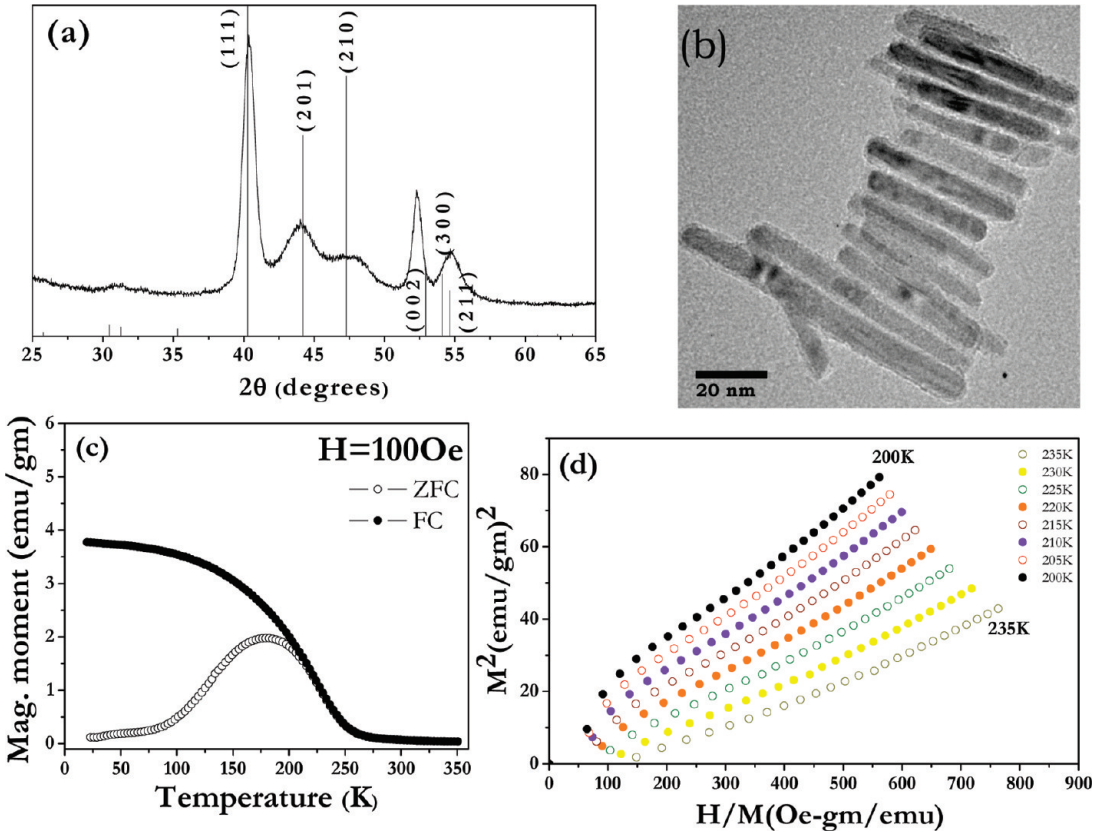

Figure 3. (a) PXRD pattern of a phase-pure Fe_2P nanoparticle sample indexed to reference pattern PDF #85-1727. (b) TEM image of the Fe_2P nanorods. (c) Magnetization *vs* temperature data on Fe_2P nanorods. (d) Arrott plot measurements to determine T_C.

cooled (ZFC) and field-cooled (FC) measurement protocols at an applied field of 100 Oe. These data are shown in Figure 3c. Both curves show a sharp rise in susceptibility below 250 K, consistent with the onset of ferromagnetic order. To determine the exact Curie temperature (T_C) of the Fe_2P sample, *M versus H* curves were collected at temperatures around the expected the T_C (200−235 K) and plotted as M^2 *versus* H/M (Arrott plots, Figure 3d). For a second-order phase transition, such as the magnetic ordering transition observed here, Arrott plots yield a set of parallel lines with the curve corresponding to $T = T_C$ passing through the origin.[22] Our data show that the 215 and 220 K measurements pass on either side of the origin, suggesting the T_C for the nanorods occurs between these values. This agrees with the transition temperature for bulk Fe_2P (217 K) reported by Fujii and co-workers.[23]

ZFC measurements enable superparamagnetic behavior, characteristic of nanoscale ferromagnets, to be assessed. The superparamagnetic transition or blocking temperature, T_B, refers to the temperature at which the thermal energy dominates the magnetic energy over the time scale of the measurement, that is, where magnetic relaxation of the nanoscale ferromagnets is faster than the measuring time and the coercive field drops to zero. For a nanoparticle system, T_B typically increases with increased magnetic volume and magne-

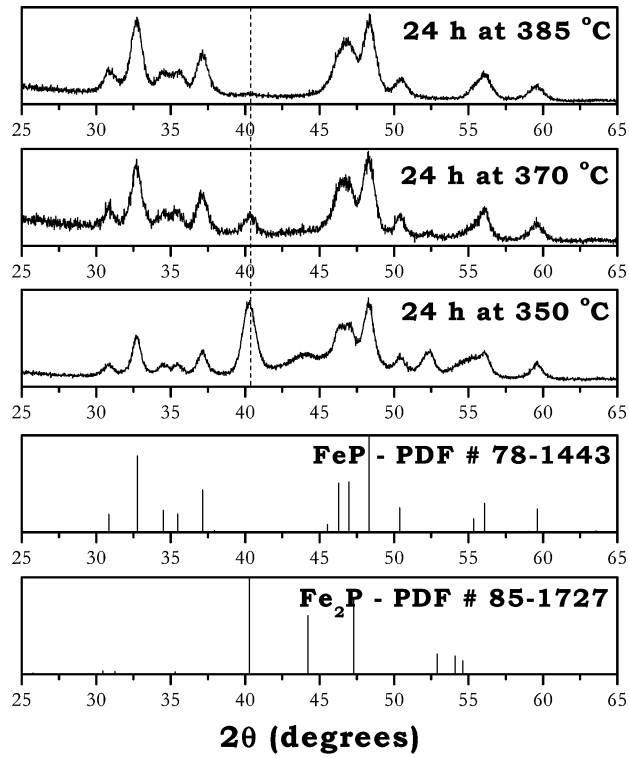

Figure 4. PXRD patterns depicting the effect of temperature on the distribution of FeP and Fe_2P in the product produced by PATH-A (Scheme 1). The characteristic peak of Fe_2P is marked with a dotted line.

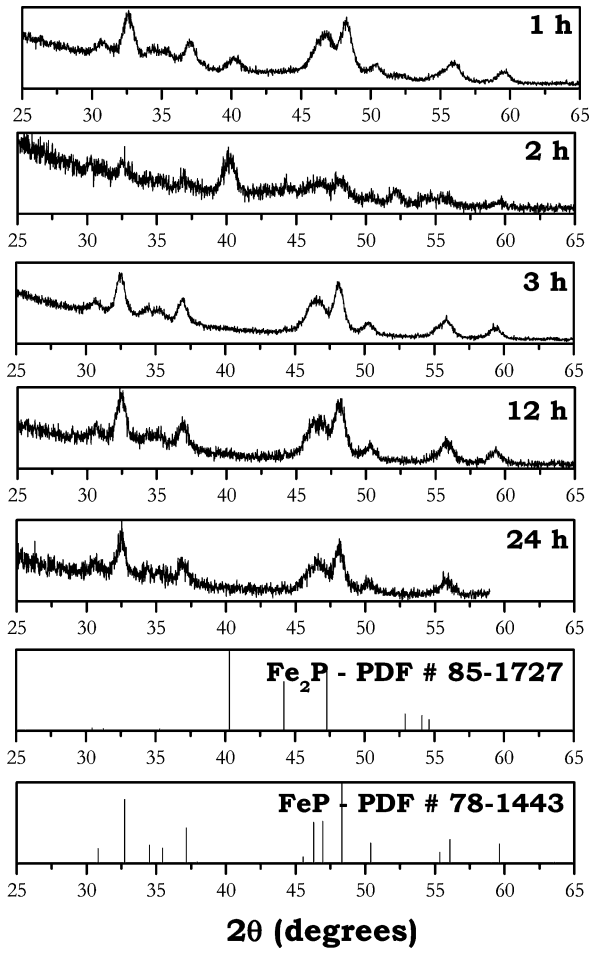

Figure 5. PXRD patterns of the products from PATH-B (Scheme 1) as a function of time at 350 °C.

tocrystalline anisotropy. The ZFC measurement (Figure 3c) exhibits a peak around 179 K, corresponding to the blocking temperature (T_B) for the *ca.* 8 × 70 nm Fe_2P nanorods, and consistent with the expected behavior of a nanoscale ferromagnet. On the basis of these results, we believe it is possible that studies on nanoscale Fe_2P reporting T_B values[2,11] greater than T_C and/or where hysteresis loops[14] are observed at temperatures above T_C could be on samples contaminated by metallic or oxidized iron species, or possibly Fe_3P (T_C = 716 K). These data emphasize the unreliability of PXRD for purity assessment in cases where ferromagnetic impurities are likely.[24] In the present case, the attraction of the material to a stir bar at room temperature suggests the presence of common Fe-based impurities and provides an easy check for these secondary phases. This is particularly valuable for the phosphides because the presence of TOP as a capping ligand precludes using chemical analysis for evaluation of phase-pure samples; the materials all appear to be phosphorus-rich.[25]

Effect of Temperature on the Final Product: Reaction Series IV and V. Encouraged by our success in preparing phase-pure Fe_2P, we next set out to synthesize phase-pure FeP. To be able to make the phosphorus-rich product (FeP), we surmised that a larger quantity of reactive phosphorus is needed and that this could be achieved by increasing the temperature, enabling complete conversion of Fe nanoparticles to FeP nanoparticles without Fe_2P impurities. A series of reactions, similar in conditions to reaction series I, were carried out at 370 °C (reaction series IV) and 385 °C (reaction series V) and the products analyzed by PXRD (Supporting Information). The results were similar to those observed in reaction series I, that is, longer heating times reduced, but failed to completely eliminate Fe_2P. However, increasing temperature did significantly decrease the amount of Fe_2P (Figure 4), as assessed from the intensity of the (111) reflection of Fe_2P (40.2° 2θ). This is consistent with our hypothesis that more of the TOP is activated, yielding a higher concentration of phosphorus available for conversion and resulting in the formation of phosphorus-rich product (FeP) in higher quantities. In attempts to drive the reaction to completion, a second injection of 10.0 mL of TOP, carried out halfway through a 24 h reaction at 370 °C, was attempted but also failed to completely eliminate Fe_2P impurities (Supporting Information).

Injection of Fe Nanoparticles into Preheated TOP: Reaction Series VI. In all of the reactions previously discussed, TOP at room temperature was injected into the Fe nanoparticle system at 200 °C and the temperature was ramped up to target. Although longer reaction times yielded FeP as the dominant product, phase-pure FeP remained elusive. We hypothesized that the gradual availability of active phosphorus required for conversion in the synthesis enables particle growth simultaneous with the transformation of intermediary Fe_2P to FeP. The larger the particles, the larger the kinetic barrier to diffusion and therefore transformation. Alternatively (or concomitantly), a protective layer of FeP may form on the outside of Fe_2P, preventing complete conversion.

In an attempt to circumvent these potential effects, we decided to introduce the iron nanoparticles at the reaction temperature, ensuring that the reaction was conducted entirely under conditions thermodynamically favorable for FeP formation. To achieve this, a variation in the synthesis scheme was introduced wherein Fe nanoparticles at 200 °C were cannulated into preheated TOP (Scheme 1, PATH-B). A series of reactions were carried out by this cannulation method at 350 °C, and the isolated products were analyzed by PXRD and evaluated as a function of heating time. The PXRD patterns (Figure 5) clearly reveal the formation of a phase-pure product (FeP) within 24 h (*i.e.*, Fe_2P was not detected). The PXRD patterns of the 1 and 2 h samples have a clear peak at 40.2° (2θ), characteristic of Fe_2P, and a slight rise in the background at 40° in the patterns of the 3 and 12 h samples suggests residual Fe_2P may be present there, as well.

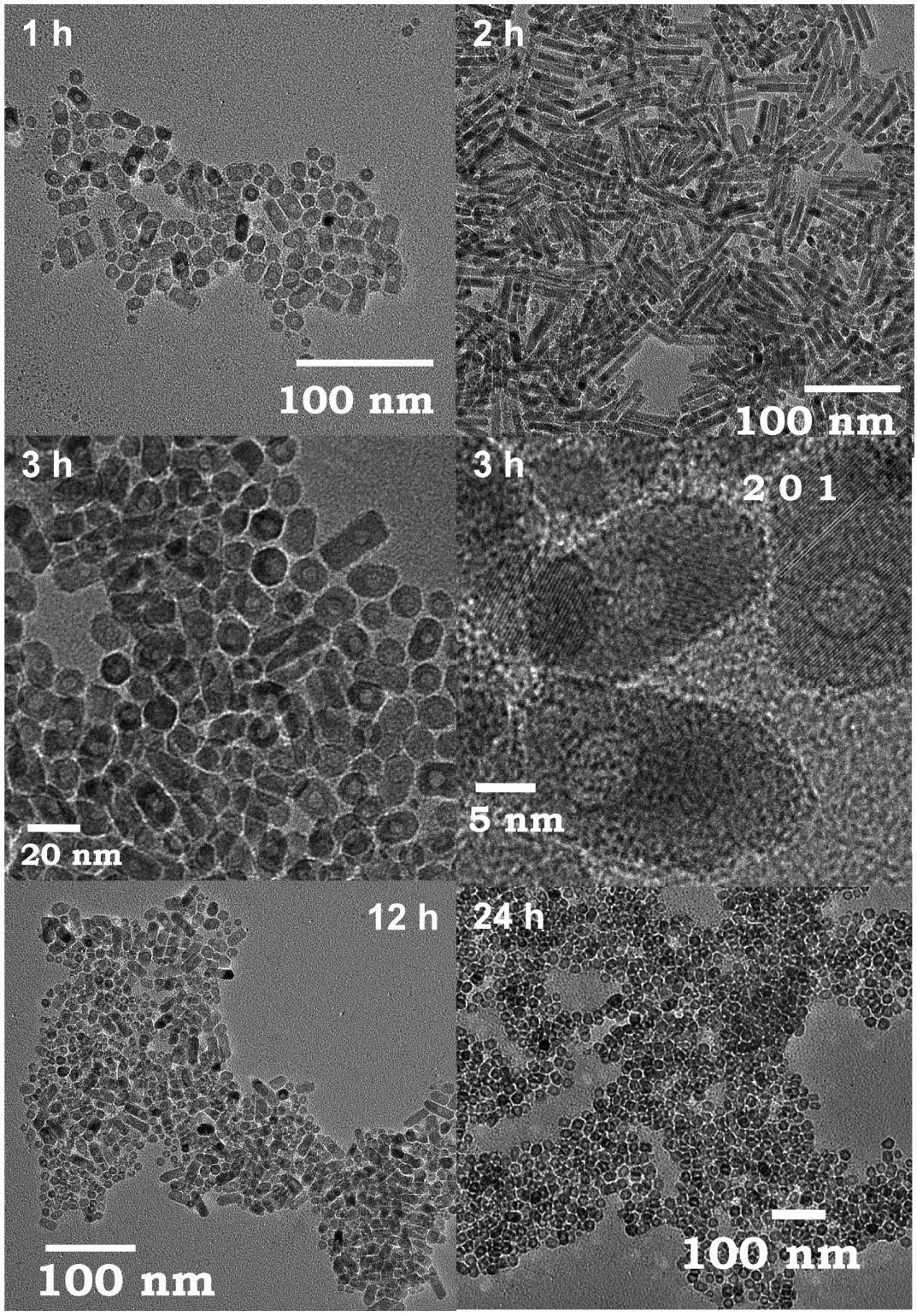

Figure 6. Effect of heating time (350 °C) on the morphology of the product generated by PATH-B (Scheme 1).

Clear changes in particle morphology mirror the changes in the PXRD patterns, as shown in Figure 6. At very short times (1 h) after cannulation, conversion to phosphides presumably takes place by a topotactic mechanism, resulting in near spherical particles and very short rods. Increased heating times result in rod formation (2 h), and further heating (3 and 12 h) results in the shortening of the nanorods. In particular, the 3 h sample was found to consist of near spherical particles with an average size of 16.5 nm and rods whose length and width ranged from 40−80 and 12−18 nm, respectively. HRTEM reveals lattice fringes with spacing of 2.326 Å, corresponding to the (201) planes of FeP. Prolonged heating (24 h) resulted in the disappearance

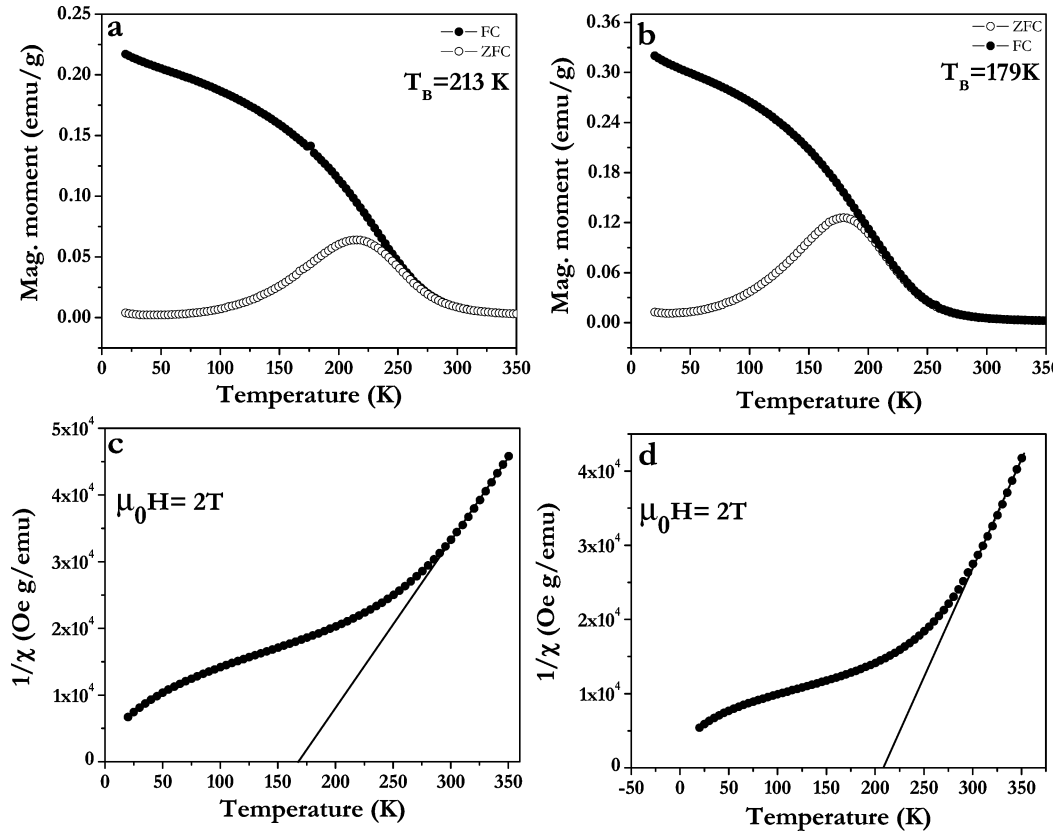

Figure 7. ZFC/FC curves of Fe_xP nanoparticles prepared by PATH-B (Scheme 1), measured at H = 100 Oe, for (a) 3 h sample and (b) 12 h sample. Inverse susceptibility *vs* temperature plots for (c) 3 h sample and (d) 12 h sample, indicating the presence of a ferromagnetic component. The straight line in (c) and (d) indicates the extrapolation of the high temperature inverse susceptibility used to estimate the Weiss interaction temperature.

of the nanorods, and the system was completely made up of near spherical particles. These all exhibited spherical hollows, indicative of the Kirkendall effect. Despite prior reports of FeP nanorods in the literature,[10,12] under the conditions employed here, the dominant morphology is clearly spherical. On the basis of these data, it appears that the transformation of spherical Fe nanoparticles to hollow spheres of FeP may occur *via* multiple pathways, including direct (topotactic) transformation as well as proceeding *via* Fe_2P as an intermediary phase that adopts an anisotropic morphology. As Fe_2P transforms to FeP, the Fe_2P rods become shorter, ultimately becoming spherical.

The presence of residual Fe_2P in 3 and 12 h samples is also suggested by magnetic susceptibility results (Figure 7). Both curves exhibit an increase in susceptibility below 250 K and have estimated T_B values of 213 K (3 h) and 179 K (12 h). This ferromagnetic response is unexpected because FeP itself is a metamagnet with no net ferromagnetic moment and a Néel temperature (T_N) of 115 K. In order to clarify the nature of the putative impurity phase, the magnetizations were measured as a function of temperature at a higher field, 2 T. This exceeds the saturation field for Fe_2P, which results in complete saturation of any ferromagnetic moments arising from this impurity phase. A plot of inverse susceptibility against temperature (Figure 7c,d) gives information about the nature of the interactions in the sample. The positive Weiss constant fit for both samples at high temperatures confirms the presence of ferromagnetic interactions in the nanoparticles. On the basis of the similarity of Figure 7a,b to Figure 3c, we think it is likely that the magnetic response is due to untransformed Fe_2P. Comparing the low temperature FC magnetizations in Figures 3c and a, we estimate that the possible Fe_2P impurity phase represents no more than 5% of the total mass, which may explain why it is difficult to observe in routine PXRD. Moreover, the blocking temperature of the 3 h sample (213 K) is higher than that of the 12 h sample (179 K), suggesting larger ferromagnetic particles in the former case. If the mechanism of conversion involves Fe → Fe_2P → FeP, the effective particle size of Fe_2P should decrease during conversion, resulting in a lower blocking temperature for the 12 h sample, as we have observed here.

Generation of Phase-Pure FeP Nanoparticles and Magnetic Properties. To ensure phase-pure samples for magnetic susceptibility analysis, the cannulation reaction (PATH-B, Scheme 1) was conducted for 24 h at a higher temperature, 370 °C. As shown in Figure 8, the PXRD pattern reveals no discernible impurities, and the particles are uniformly spherical (14.9 ± 1.2 nm) according to TEM. Magnetic measurements conducted at 2 T (Figure 8c) are consistent with a paramagnetic response

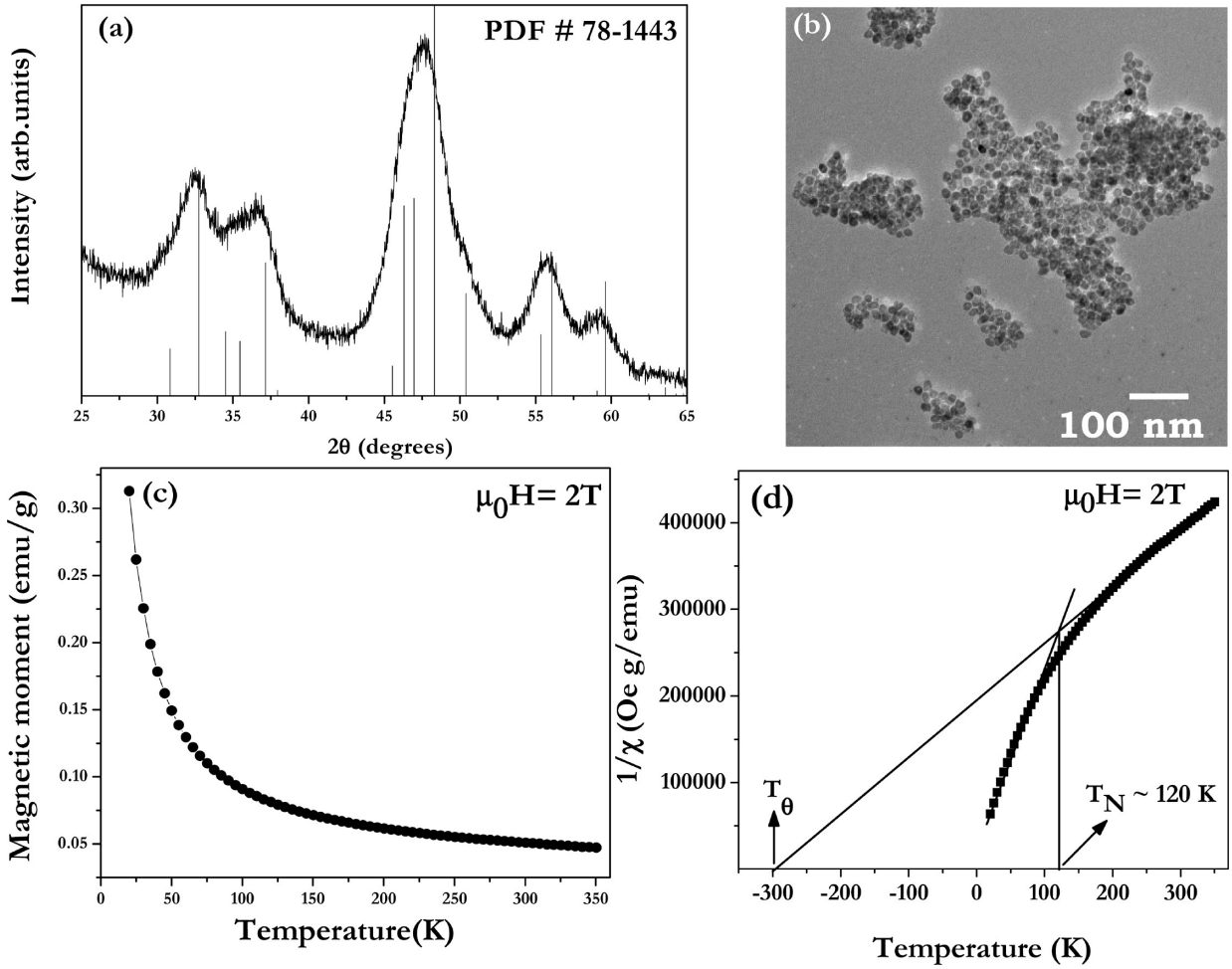

Figure 8. (a) PXRD pattern of a phase-pure FeP nanoparticle sample prepared by optimizing the synthetic conditions in PATH-B compared to the FeP reference pattern. (b) TEM image of the near spherical FeP nanoparticles; a high resolution image is included in Supporting Information. (c) Magnetization *vs* temperature measurements of phase-pure FeP measured in a field of 2 T. (d) Corresponding $1/\chi$ *vs* *T* plot.

from 350 to 125 K, with a larger rate of increase in the magnetization at temperatures below 125 K. While there is some curvature in the inverse susceptibility plotted against temperature, a linear extrapolation of the high temperature portion of the $1/\chi$ *versus* *T* data (Figure 8d) yields a negative Weiss constant of −300 K, suggesting the presence of antiferromagnetic interactions. Although there is no clear magnetic anomaly in these data to indicate the onset of antiferromagnetic order in the FeP nanoparticles, we propose that the increase in magnetization above the paramagnetic contribution at low temperature may reflect an incomplete cancellation of the antiferromagnetic spins in these nanoparticles. Accordingly, T_N for the system was estimated from the intersection of the two slopes extrapolated to the temperature axis (Figure 8d). On the basis of this analysis, the approximate value of T_N for the FeP nanoparticles was 120 K, which is close to the reported value for bulk FeP (115 K).[26] The absence of ferromagnetic contributions is consistent with earlier reports on 5 nm FeP nanoparticles[8] and FeP nanowires.[12] It can thus be concluded that the prior reports of ferromagnetism in FeP[10,13] may reflect the presence of secondary phases in these samples, such as Fe, iron oxides, or Fe_2P.

Intriguingly, the magnetic data suggest much stronger interactions are present in the 15 nm hollow nanoparticles presented here than we previously observed in 5 nm spherical FeP nanoparticles.[8] For the 5 nm spherical FeP nanoparticles, the deviation from linearity in the $1/\chi$ *versus* *T* plot was much weaker and occurs near 75 K, well below the reported bulk T_N. Additionally, the Weiss constant is much smaller (−20 K).[8] The difference is likely a function of the particle size. The helimagnetic structure of FeP has a repeat distance of nearly 3 nm,[26] and there may be a critical particle volume needed to achieve long-range order.

CONCLUSIONS

The selection of phase (FeP or Fe_2P) in the transformation of Fe nanoparticles to iron phosphides by high temperature treatment with trioctylphosphine is a sensitive function of heating time, temperature, reaction concentration, and even order of reagent addition. In

all cases, Fe_2P is found to form at short reaction times and adopt a rod morphology, occasionally with hollows characteristic of the Kirkendall effect. Moreover, sufficiently high concentrations of Fe enable production of phase-pure Fe_2P. At suitably long times and high temperatures, Fe_2P transforms to FeP and adopts a spherical morphology (again with hollows); however, driving this reaction to completion is challenging, suggesting some kind of kinetic barrier. We speculate that FeP formation by conversion from Fe_2P is often incomplete due to decreased ion mobility from the core as the FeP shell thickness increases. This is alleviated by rapid reaction of iron and TOP at temperatures that thermodynamically favor FeP, perhaps due to some degree of topotactic transformation of Fe to FeP in addition to the Fe_2P to FeP transformation. It should be noted that the transformations of Fe to Fe_2P or Fe_2P to FeP do not appear to be topotactic and are accompanied by a drastic change in morphology (sphere to rod, rod back to sphere). Importantly, when care is taken to prepare phase-pure FeP and Fe_2P, the magnetic properties observed are in line with expectations arising from the behavior of bulk phases. On the basis of this study, prior reports of unexpected magnetic behavior in FeP and Fe_2P nanoparticles[10,11,13,14] can potentially be attributed to ferromagnetic impurities, which can be expected to dominate the response, even when present in small (not detectible by PXRD) quantities.

METHODS

Chemicals. Iron pentacarbonyl (99.999% metal basis purity) was purchased from Sigma Aldrich and was stored in a refrigerator maintained at −20 °C in a glovebox. Trioctylphosphine (97%) was purchased from STREM Chemicals and was stored under argon in a glovebox. 1-Octadecene (90% tech.) was purchased from Sigma Aldrich and oleylamine (C_{18} content 80−90%) from ACROS; chloroform (99%) and pyridine (99%) were purchased from Fisher Scientific; ethanol (200 proof) was purchased from Decon Laboratories Inc. All chemicals were used as received.

Synthesis. All reactions were carried out under an argon atmosphere using standard Schlenk line techniques. The synthesis is outlined in Scheme 1 and involves two steps: (i) synthesis of monodisperse Fe nanoparticles by following a method published by Sun and co-workers,[19] and (ii) subsequent conversion of Fe nanoparticles into phosphides by reacting them with TOP. Fe nanoparticles are synthesized by injecting 0.2−1.0 mL of $Fe(CO)_5$ into a degassed system of 20.0 mL of octadecene (solvent) and 0.3 mL of oleylamine (stabilizing ligand) at 200 °C. The system is aged at 200 °C for 20 min. Conversion of Fe nanoparticles is initiated by injecting TOP (2.5−26.5 mL) into the Fe nanoparticles system at 200 °C followed by aging at temperatures of 350, 370, or 385 °C for periods ranging from 1 to 72 h (PATH-A). In some cases, conversion was initiated by cannulating the Fe nanoparticles at 200 °C into TOP maintained at temperatures >300 °C (PATH-B). Isolation of the final products was carried out, after returning the system to room temperature, by addition of excess ethanol (20−50 mL), followed by centrifugation. The isolated particles were then sonicated for about 5−10 min with small quantities of chloroform (1−3 mL) to create a dispersion, followed by addition of an antisolvent (ethanol) and centrifugation. This process was carried out 2−3 times followed by drying under vacuum to yield a free-flowing powder of Fe_xP nanoparticles.

Characterization Techniques. Powder X-ray diffraction (PXRD) was carried out on a Rigaku diffractometer (RU200B) using the Kα line of a Cu rotating anode source (40 kV, 150 mA). Samples were deposited onto a zero background quartz holder with a thin layer of grease, and data were acquired in the 2θ range of 25−65° with a step size of 0.02°. PXRD patterns were processed using Jade 5.0 software and compared to powder diffraction files (PDF's) from the International Center for Diffraction Data (ICDD) database.

Electron microscopy and energy dispersive spectroscopy (EDS) were performed using a JEOL FasTEM 2010 electron microscope operated at a voltage of 200 kV and a beam current of 107−108 μA with a coupled EDS detector (EDAX Inc.). The images were captured using Amtv600 software provided by the Advanced Microscopy Techniques Corporation. Samples for TEM analysis were prepared by depositing a drop of a chloroform or pyridine nanoparticle dispersion onto a carbon-coated 200 mesh Cu grid, followed by air-drying.

Magnetic susceptibility measurements were carried out using a SQUID magnetometer (MPMS-5S) with a sensitivity of 10^{-7}−10^{-6} emu from Quantum Design. Samples for magnetic susceptibility were prepared by sealing the powder sample in a quartz tube under vacuum. The temperature-dependent dc magnetization measurements were measured using a zero-field-cooled (ZFC) protocol from 20 to 350 K in a magnetic field of 100 Oe. The measurement is then repeated over the same temperature range and magnetic field using a field-cooled (FC) protocol. FC measurements were also carried out on FeP samples under an applied field of 2 T in the temperature range of 20 to 350 K. Arrott plots, a series of M^2 *versus* H/M lines, were generated from M *versus* H curves of Fe_2P nanorods collected at several temperatures (200−235 K) near the expected Curie temperature.

Acknowledgment. We thank Y. Liu of the Wayne State University Central Instrument Facility (WSU-CIF) for assistance with TEM. This work was supported by the National Science Foundation (DMR-331769) and the donors of the Petroleum Research Fund, administered by the American Chemical Society (46160-G10). Electron microscope was acquired in the WSU-CIF on a JEOL 2010F purchased under NSF Grant DMR-0216084.

Note added after ASAP publication: Because of a production error the ASAP paper was initially published without author comments. The corrected version was published on the Web on August 6, 2009.

Supporting Information Available: High resolution TEM image of Fe nanoparticles; histogram depicting the size distribution of the Fe nanoparticle precursors; PXRD pattern of Fe nanoparticles; PXRD patterns of products from reaction series IV and V; PXRD pattern of the product from multiple injections of TOP; additional TEM images of Fe_2P nanorods; HRTEM and EDS data on phase-pure FeP nanoparticles. This material is available free of charge *via* the Internet at http://pubs.acs.org.

REFERENCES AND NOTES

1. Hullinger, F. Crystal Chemistry of the Chalcogenides and Pnictides of the Transition Metals. *Struct. Bonding* **1968**, *4*, 83–229.
2. Luo, F.; Su, H.-L.; Song, W.; Wang, Z.-M.; Yan, Z.-G.; Yan, C.-H. Magnetic and Magnetotransport Properties of Fe_2P Nanocrystallites *via* a Solvothermal Route. *J. Mater. Chem* **2004**, *14*, 111–115.
3. Tegus, O.; Brück, E.; Buschow, K. H. J.; de Boer, F. R. Transition-Metal-Based Magnetic Refrigerants for Room-Temperature Applications. *Nature* **2002**, *415*, 150–152.
4. Brock, S. L.; Perera, S. C.; Stamm, K. L. Chemical Routes for Production of Transition-Metal Phosphides on the

Nanoscale: Implications for Advanced Magnetic and Catalytic Materials. *Chem.—Eur. J.* **2004**, *10*, 3364–3371.
5. Feichter, S.; Tributsch, H.; Evain, M.; Brec, R. γ-FeP_4, A New Photosensitive Semiconductor. *Mater. Res. Bull.* **1987**, *22*, 543–549.
6. Blanchard, P. E. R.; Grosvenor, A. P.; Cavell, R. G.; Mar, A. X-ray Photoelectron and Absorption Spectroscopy of Metal-Rich Phosphides M_2P and M_3P (M = Cr-Ni). *Chem. Mater.* **2008**, *20*, 7081–7088.
7. Grosvenor, A. P.; Cavell, R. G.; Mar, A., Bonding and Electronic Structure of Phosphides, Arsenides and Antimonides by X-ray Photoelectron Spectroscopy. In *Structure and Bonding*; Springer: Berlin, 2009; available online.
8. Perera, S. C.; Fodor, P. S.; Tsoi, G. M.; Wenger, L. E.; Brock, S. L. Application of De-silylation Strategies to the Preparation of Transition Metal Pnictide Nanocrystals: The Case of FeP. *Chem. Mater.* **2003**, *15*, 4034–4038.
9. Brock, S. L.; Senevirathne, K. Recent Developments in Synthetic Approaches to Transition Metal Phosphide Nanoparticles for Magnetic and Catalytic Applications. *J. Solid State Chem.* **2008**, *181*, 1522–1559.
10. Park, J.; Koo, B.; Yoon, K. Y.; Hwang, Y.; Kang, M.; Park, J.-G.; Hyeon, T. Generalized Synthesis of Metal Phosphide Nanorods *via* Thermal Decomposition of Continously Delivered Metal-Phosphine Complexes Using a Syringe Pump. *J. Am. Chem. Soc.* **2005**, *127*, 8433–8440.
11. Park, J.; Koo, B.; Hwang, Y.; Bae, C.; An, K.; Park, J.-G.; Park, H. M.; Hyeon, T. Novel Synthesis of Magnetic Fe_2P Nanorods from Thermal Decomposition of Continously Delivered Precursors Using a Syringe Pump. *Angew. Chem., Int. Ed.* **2004**, *43*, 2282–2285.
12. Qian, C.; Kim, F.; Ma, L.; Tsui, F.; Yang, P.; Liu, J. Solution-Phase Synthesis of Single-Crystalline Iron Phosphide Nanorods/Nanowires. *J. Am. Chem. Soc.* **2004**, *126*, 1195–1198.
13. Chen, J.-H.; Tai, M.-F.; Chi, K.-M. Catalytic Synthesis, Characterization and Magnetic Properties of Iron Phosphide Nanowires. *J. Mater. Chem.* **2004**, *14*, 296–298.
14. Kelly, A. T.; Rusakova, I.; Ould-Ely, T.; Hofmann, C.; Lüttge, A.; Whitmire, K. H. Iron Phosphide Nanostructures Produced from a Single-Source Organometallic Precursor: Nanorods, Bundles, Crosses, and Spherulites. *Nano Lett.* **2007**, *7*, 2920–2925.
15. Henkes, A. E.; Vasquez, Y.; Schaak, R. E. Converting Metals into Phosphides: A General Strategy for the Synthesis of Metal Phosphide Nanocrystals. *J. Am. Chem. Soc.* **2007**, *129*, 1896–1897.
16. Henkes, A. E.; Schaak, R. E. Trioctylphosphine: A General Phosphorus Source for the Low-Temperature Conversion of Metals into Metal Phsophides. *Chem. Mater.* **2007**, *19*, 4234–4242.
17. Henkes, A. E.; Schaak, R. E. Template-Assisted Synthesis of Shape-Controlled Rh_2P Nanocrystals. *Inorg. Chem.* **2008**, *47*, 671–677.
18. Vasquez, Y.; Henkes, A. E.; Bauer, J. C.; Schaak, R. E. Nanocrystal Conversion Chemistry: A Unified and Materials-General Strategy for the Template-Based Synthesis of Nanocrystalline Solids. *J. Solid State Chem.* **2008**, *181*, 1509–1523.
19. Peng, S.; Wang, C.; Xie, J.; Sun, S. Synthesis and Stabilization of Monodisperse Fe Nanoparticles. *J. Am. Chem. Soc.* **2006**, *128*, 10676–10677.
20. Shao, H.; Lee, H.; Huang, Y.; Ko, I.; Kim, C. Control of Iron Nanoparticles Size and Shape by Thermal Decomposition Method. *IEEE Trans. Magn.* **2005**, *41*, 3388–3390.
21. Chiang, R. C.; Chiang, R.-T. Formation of Hollow Ni_2P Nanoparticles Based on the Nanoscale Kirkendall Effect. *Inorg. Chem.* **2007**, *46*, 369–371.
22. Mukherjee, S.; Rayachaudhuri, P.; Nigam, A. K. Critical Behavior in $La_{0.5}Sr_{0.5}CoO_3$. *Phys. Rev. B* **2000**, *61*, 8651–8653.
23. Fujii, H.; Uwatoko, Y.; Motoya, K.; Ito, Y.; Okamoto, T. Neutron Scattering Investigation of Itinerant Electron System Fe_2P. *J. Phys. Soc. Jpn.* **1988**, *57*, 2143–2153.
24. Aitken, J. A.; Tsoi, G. M.; Wenger, L. E.; Brock, S. L. Phase Segregation of MnP in Chalcopyrite Dilute Magnetic Semiconductors: A Cautionary Tale. *Chem. Mater.* **2007**, *19*, 5272–5278.
25. Senevirathne, K.; Burns, A. W.; Bussel, M. E.; Brock, S. L. Synthesis and Characterization of Discrete Nickel Phosphide Nanoparticles: Effect of Surface Ligation Chemistry on Catalytic Hydrodesulfurization of Thiophene. *Adv. Funct. Mater.* **2007**, *17*, 3933–3939.
26. Felcher, G., P; Smith, F. A.; Bellavance, D.; Wold, A. Magnetic Structure of Iron Monophosphide. *Phys. Rev. B* **1971**, *3*, 3046–3052.